



## Low-temperature combustion of chlorinated hydrocarbons over CeO<sub>2</sub>/H-ZSM5 catalysts

Beatriz de Rivas, Carmen Sampedro, Rubén López-Fonseca\*, Miguel Ángel Gutiérrez-Ortiz, Jose Ignacio Gutiérrez-Ortiz

Chemical Technologies for Environmental Sustainability Group, Department of Chemical Engineering, Faculty of Science and Technology, Universidad del País Vasco/EHU, PO Box 644, E-48080 Bilbao, Spain

### ARTICLE INFO

#### Article history:

Received 19 September 2011  
Received in revised form 1 December 2011  
Accepted 16 December 2011  
Available online 27 December 2011

#### Keywords:

Chlorinated VOCs  
Catalytic oxidation  
1,2-Dichloroethane  
Supported cerium oxide catalyst  
H-ZSM5 zeolite

### ABSTRACT

The performance of various CeO<sub>2</sub>/H-ZSM5 catalysts was evaluated for the oxidation of one of the most common chlorinated pollutants found in waste streams, namely 1,2-dichloroethane. The supported samples with varying CeO<sub>2</sub> loading (6–50 wt.%) were prepared by impregnation and subsequently calcined at 550 °C. Structural, morphological and physico-chemical changes caused by the CeO<sub>2</sub> addition were analysed by X-ray diffraction, transmission electronic microscopy, N<sub>2</sub>-physisorption, temperature-programmed desorption of ammonia and temperature-programmed reduction with hydrogen. The enhancement of the catalytic behaviour of the resulting samples with respect to plain H-ZSM5 could be accounted for on the basis of the synergetic role played by oxygen mobility and acid sites. Hence, an optimum cerium loading of 11 wt.% was found with a *T*<sub>50</sub> value around 210 °C. At 350 °C, where conversion of the chlorinated feed is about 99%, the major oxidation products were carbon oxides and hydrogen chloride with a reduced presence of chlorinated by-products and molecular chlorine. A relatively good catalytic stability was noticed during 80 h time on line.

© 2011 Elsevier B.V. All rights reserved.

### 1. Introduction

The increased production and application of chlorinated volatile organic compounds (VOCs) have caused increased concerns over proper disposal and control of these hazardous waste materials. These compounds have a high chemical and thermal stability, and tend to accumulate in the environment. Besides causing localised odour problems, these pollutants are responsible for the increase in ground-level ozone concentrations and the formation of secondary organic aerosols as well. Moreover, some compounds have a carcinogenic, teratogenic or mutagenic character. For this reason, in recent years legislation has been introduced in many countries setting very low emissions limits in process exhaust gases [1].

Chlorinated VOCs have been produced commercially and used for many purposes by the chemical industry including the manufacture of herbicides, plastics, and solvents. Uses outside the chemical industry include solvent degreasing in the automotive and aerospace industries, and dry cleaning solvents in the garment industries and precision solvent cleaning in the electronic industries. When VOC emissions cannot be avoided, they ought to be controlled by an appropriate end-of-pipe-device. If there

is no interest in recovering VOCs they are usually destroyed by deep oxidation. However, as the VOC concentration is usually very low (below 1000 ppm), direct combustion may not be appropriate. In conventional incineration methods temperatures exceeding 700 °C are required to obtain complete decomposition. This would require a large amount of extra fuel to maintain the flame temperature and may produce toxic substances and NO<sub>x</sub>. Furthermore, the combustion of chlorinated hydrocarbons presents additional complications. For instance, chlorine-containing materials are known to inhibit flame propagation and have low heats of combustion. As a result, development of low-temperature (in the range 300–550 °C) processes for chlorinated waste disposal can offer significant improvements over traditional thermal oxidation [2]. Catalytic deep oxidation is more selective and, as it requires less heating, is more cost effective than direct combustion for treating oxygen-containing waste gases. As large gas volumes have to be typically treated, this catalytic approach has to be performed at very high space velocity (>10,000 h<sup>-1</sup>) and thus requires a very active catalyst. A catalytic combustion process, if properly designed, must lead to the complete destruction of all kinds of chlorinated VOC including the harmful by-products, which can be produced by an incomplete destruction of the starting chlorocarbon.

Supported noble-metal catalysts as well as (supported) metal oxide catalysts are commercially applied for the oxidation process. Alumina is most frequently employed as a carrier. Noble metals

\* Corresponding author. Tel.: +34 94 6015985; fax: +34 94 6015963.  
E-mail address: [ruben.lopez@ehu.es](mailto:ruben.lopez@ehu.es) (R. López-Fonseca).

are powerful oxidation catalysts, but can easily form inorganic chlorides, with deactivation as a likely consequence. Furthermore, noble-metal chloride species could also cause chlorination of organic compounds besides its oxidation [3,4]. Additional disadvantages of this type of catalysts are associated with their high cost and limited availability. Metal oxide catalysts, such as chromium, vanadium and copper oxides, are reported to be suitable for this process as well, although the lower activity and volatilisation of metalloxychlorides can be serious drawbacks [3]. Thus substantial efforts are currently being made to develop alternative catalysts with a comparable performance.

Recently, ceria-based bulk oxides have shown promising results in the oxidation of chlorinated VOCs owing to their remarkable redox properties (based on its high oxygen-storage capacity and facile cycle of  $\text{Ce}^{4+}/\text{Ce}^{3+}$ ), thermal stability and resistance to Cl-poisoning [5–9]. Hence, it seems reasonable to expect that the overall catalytic behaviour of the resulting Ce catalyst could be noticeably improved by suitably supporting this active phase on a carrier. Moreover, it was previously demonstrated that the support itself can play a relevant role in enhancing the conversion of the chlorinated hydrocarbons [10]. This promoting effect has been typically associated with the acidic properties. In this work our attention was focused on the use of H-zeolites as an appropriate support. There is a wide range of zeolite structures available with variable aluminium concentrations, enabling zeolites with specific properties to be selected as catalyst support. The selection of H-ZSM5 zeolite for this work was justified on the basis of previous reports where a number of zeolites including H-Y, H-ZSM5, H-MOR and H-BETA were examined in the oxidative decomposition of chlorinated hydrocarbons [11–13]. The better catalytic behaviour was related to its relatively high internal surface area, strong acidity and three-dimensional channel system. Moreover, when compared with conventional (alumina and silica) supports Gutierrez-Ortiz et al. [14] found a highly active behaviour for H-ZSM5 supported  $\text{Mn}_2\text{O}_3$  catalysts in the oxidation of dichloromethane and trichloroethylene. Accordingly, Scire et al. [15] observed a better catalytic behaviour for supported Pt catalysts when H-ZSM5 zeolite was used as carrier with respect to H-BETA and alumina in the combustion of chlorobenzene. In this sense, Rachapudi et al. [16] also reported a good performance of Cr/H-ZSM5 catalysts in the destruction of vinyl chloride and trichloroethylene although a partial loss of toxic chromium was noticed.

In the present work the suitability of H-ZSM5 supported ceria catalysts for the oxidation of 1,2-dichloroethane, which was chosen as a model chlorinated VOC, was examined in a fixed-bed flow reactor. 1,2-Dichloroethane ( $\text{C}_2\text{H}_4\text{Cl}_2$ , DCE), also known as ethylene dichloride, is probably one of the most important chlorinated VOC emitted in gaseous industrial waste streams since it is used as an intermediate for the production of polyvinyl chloride, the most produced plastic in the world after polyethylene [17]. Less important uses are as a solvent in textile cleaning and metal degreasing and paint remover, a starting material for paint, varnish, and finish removers, a cleaner for upholstery and carpets, a fumigant, a lead scavenger in antiknock gasoline, and as a dispersant for plastics and elastomers such as synthetic rubber [18].

## 2. Experimental

### 2.1. Catalysts preparation

The parent ZSM-5 zeolite (Si/Al=27.3 as determined by XRF analysis [11]) was supplied by Zeolyst Corp. The supported samples were prepared by impregnation of the zeolite (10 g) with aqueous solutions ( $100\text{ cm}^3$ ) of cerium nitrate (Aldrich) for 4 h under

vacuum conditions. Five samples with varying  $\text{CeO}_2$  loadings (6, 11, 17, 26 and 50 wt.%) were obtained. These were denoted as  $\text{CeO}_2(x)/\text{H-ZSM5}$  where  $x$  is the  $\text{CeO}_2$  content. A pure ceria catalyst was used as a reference for comparative purposes. This sample was prepared by Rhodia using a proprietary precipitation route from the nitrate precursor. The samples were then dried at  $110^\circ\text{C}$  overnight followed by calcination at  $550^\circ\text{C}$  for 4 h in static air. Next, catalyst pellets with a 0.3–0.5 mm diameter were prepared by a process of compressing the oxide powders into flakes in a hydraulic press (Specac), crushing and sieving. All the samples obtained prior to catalytic activity and selectivity experiments were characterised using several analytical techniques.

### 2.2. Characterisation techniques

The metal content in the catalysts was measured by inductively coupled plasma-atomic emission spectroscopy (ICP-AES) in ARL Fisons 3410 ICP equipment. Prior to analysis, the samples were dissolved in an acid solution ( $\text{HCl} + \text{HNO}_3$ ) with small amounts of HF. Textural properties were evaluated from the nitrogen adsorption-desorption isotherms, determined at  $-196^\circ\text{C}$  with a Micromeritics ASAP 2010 apparatus. The adsorption data recorded from the amount of  $\text{N}_2$  physisorbed at different relative pressures were treated with the full BET equation. The 't-plot' method was applied in order to obtain an estimation of the microporous volume ( $V_{\text{micro}}$ ) and surface area ( $S_{\text{micro}}$ ), and to determine the external surface area ( $S_{\text{ext}}$ ).

X-ray diffraction (XRD) studies were carried out on a X'PERT-MPD X-ray diffractometer with Cu  $K\alpha$  radiation ( $\lambda = 1.5406\text{ \AA}$ ) and Ni filter. The X-ray tube was operated at 30 kV and 20 mA. Samples were scanned from  $5^\circ < 2\theta < 80^\circ$  and the X-ray diffraction line positions were determined with a step size of  $0.02^\circ$  and counting time of 2.5 s per step. Transmission electron microscopy (TEM) investigations were performed using a Philips CM200 microscope equipped with LaB6 crystal as electron source and operating at 200 kV. Bright field images were acquired using a high resolution CCD camera. Drops of emulsions, created by sonication of the powder samples in ethanol, were deposited on C coated Cu grids and left in air top dry.

Temperature-programmed desorption (TPD) of ammonia was performed on a Micromeritics Autochem 2920 instrument equipped with a quartz U-tube coupled to a thermal conductivity detector. Prior to adsorption experiments, the samples (40 mg) were first pre-treated in a  $5\%\text{O}_2/\text{He}$  stream at  $550^\circ\text{C}$ . Then, they were cooled down at  $100^\circ\text{C}$  in a He flow ( $20\text{ cm}^3\text{ min}^{-1}$ ). Later, the  $\text{NH}_3$  adsorption step was performed by admitting a flow of  $10\%\text{NH}_3/\text{He}$  at  $100^\circ\text{C}$  up to saturation. Subsequently, the samples were exposed to a flow of helium ( $50\text{ cm}^3\text{ min}^{-1}$ ) for 1 h at  $100^\circ\text{C}$  in order to remove reversibly and physically bound ammonia from the surface. Finally, desorption was carried out from 100 to  $550^\circ\text{C}$  at a heating rate of  $10^\circ\text{C min}^{-1}$  in a He stream ( $50\text{ cm}^3\text{ min}^{-1}$ ). This temperature was maintained for 120 min until the adsorbate was completely desorbed. The amount of gases desorbed was determined by time integration of the TPD curves. The gas stream at the exit was on-line analysed by mass spectrometry (MS) in order to verify the absence of  $\text{NO}_x$  and/or water, which could be formed as a result of ammonia oxidation during the run.

Redox behaviour was examined by temperature-programmed reduction experiments (TPR). These experiments were conducted on a Micromeritics Autochem 2920 instrument as well. Firstly, all the samples were pre-treated in an oxygen stream ( $5\%\text{O}_2/\text{He}$ ) at  $550^\circ\text{C}$  for 1 h, and then cooled down to room temperature. The reducing gas used in all experiments was  $5\%\text{H}_2$  in Ar, with a flow rate of  $50\text{ cm}^3\text{ min}^{-1}$ . The temperature range explored was from room temperature to  $950^\circ\text{C}$  with a heating rate of  $10^\circ\text{C min}^{-1}$ . This temperature was maintained for 0.5 h so as to complete the

reduction process. The water produced by reduction was trapped into a cold trap. The consumption of  $H_2$  was quantitatively measured by time integration of TPR profiles.

The amount of coke present in the used samples was determined by means of dynamic thermogravimetry using Setaram Setsys Evolution apparatus under atmospheric pressure coupled to a mass spectrometer (Pfeiffer Prisma) (TGA-MS). The mass loss and the sample temperature were continuously recorded by a computerised data acquisition system. After an isothermal step at  $150^\circ C$  the combustion of coke was carried out from  $150$  to  $900^\circ C$  at a constant heating rate of  $5^\circ C\ min^{-1}$ . The oxidant stream was  $5\% O_2/He$  ( $50\ cm^3\ min^{-1}$ ) flowing downwards onto the cylindrical sample holder. The quantification of chlorine content was evaluated by energy disperse X-ray (EDX also known as EDS, or EDAX) analysis using a JEOL JSM-6400 scanning electron microscope coupled with analysis software INCA Energy 350 from Oxford Instruments.

### 2.3. Catalyst activity determination

Catalytic tests were performed in a bench-scale fixed bed reactor (Microactivity modular laboratory system provided by PID Eng&Tech S.L.) operated at atmospheric pressure and fully monitored by computer. The reactor was made of quartz with an internal diameter of  $10\ mm$  and a height of  $300\ mm$ , in which the temperature is controlled with a thermocouple placed in the catalyst bed. Typically  $0.85\ g$  of catalyst in powdered form ( $0.3$ – $0.5\ mm$ ) was loaded. The reaction feed consisted of  $1000\ ppm$  of DCE in dry air with a total gas flow of  $500\ cm^3\ min^{-1}$ . The amount and granulometric fraction of catalyst and the total gaseous stream were chosen in order to be in true kinetic regime, namely be out of the internal and external diffusion limits, and to reach a gas hourly space velocity of  $15,000\ h^{-1}$ , which corresponds to the conditions usually met in the exhaust gases from industrial units. Catalytic activity was measured over the range  $150$ – $550^\circ C$  and conversion data were calculated by the difference between inlet and outlet concentrations. The good reproducibility of the experimental data was assessed on the basis of replicate runs. Conversion measurements and product profiles were taken at steady state, typically after  $30\ min$  on stream. Either product selectivity was calculated based on either chlorine or carbon atoms present in that product divided by the total chlorine or carbon atoms present in the product stream (expressed as %). The feed and effluent streams were analysed using an on-line 7980A Agilent Technologies gas chromatograph equipped with a thermal conductivity (CO and  $CO_2$ ) and an electron capture detector (chlorinated hydrocarbons). Analysis of HCl and  $Cl_2$  was carried out by means of ion selective electrode and titration, respectively. Further details on analytical procedures are described elsewhere [19].

## 3. Results and discussion

### 3.1. Characterisation of the catalysts

Thermogravimetric analysis was preliminary conducted in order to determine the temperature for the oxidative decomposition of the precursor salt (cerium nitrate). As a result, the activation procedure could be defined so as to obtain the desired cerium oxide ( $CeO_2$ ). Several weight losses were recorded from  $110$  to  $300^\circ C$  (not shown here), though no further change in weight was observed at higher temperatures. Thus, calcination at a temperature of at least  $300^\circ C$  was required to convert cerium nitrate into cerium oxide.

Fig. 1 shows the XRD patterns of the prepared  $CeO_2$ -zeolite catalysts calcined at  $550^\circ C$ . The patterns of the reference bulk samples ( $CeO_2$  and H-ZSM5) were also included for the sake of comparison. For all the supported samples the peaks attributed to  $CeO_2$

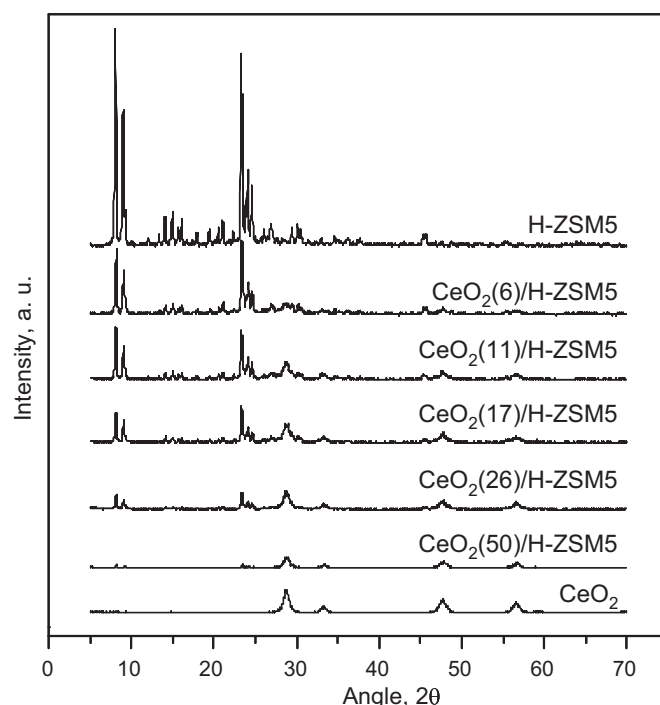


Fig. 1. XRD patterns of the  $CeO_2$ /H-ZSM5 zeolite catalysts.

with a fluorite-like structure at  $2\theta$   $23.6^\circ$ ,  $41.5^\circ$ ,  $54.4^\circ$  and  $60.1^\circ$  could be clearly observed. These peaks were increasingly intense with ceria content while the peaks associated with the H-ZSM5 zeolite markedly decreased [20]. In fact, in the case of the sample with the highest  $CeO_2$  loading ( $50\ wt.\%$ ), the signals corresponding to the crystalline support were hardly visible, which suggested that  $CeO_2$  was probably poorly dispersed on the zeolite. The mean diameter of the supported crystallites of  $CeO_2$ , calculated from the X-ray line broadening according to the Scherrer equation (Table 1), monotonically increased with  $CeO_2$  loading from  $6.3$  to  $9.9\ nm$ .

TEM images included in Fig. 2 revealed that the cerium oxide was preferentially deposited on the external zeolite surface since ceria particles were too large to enter into the H-ZSM5 framework. The fine particles were relatively spherical in shape and each particle was found to be an aggregate of nanocrystallites. As revealed by both XRD and TEM results low loadings of  $CeO_2$  ( $6$ – $11\ wt.\%$ ) led to a higher dispersion and a smaller crystallite size. In contrast, when the Ce content was larger the dispersion markedly decreased owing to the formation of conglomerates [21]. Table 1 summarises the textural properties of the zeolite catalysts in terms of specific surface area and pore volume. As a rule, it was noticed that, the more  $CeO_2$  content was impregnated, the more surface loss was observed (from about  $465\ m^2\ g^{-1}$  for the bare support to around  $270\ m^2\ g^{-1}$  for  $CeO_2(50)/H-ZSM5$ ). In line with XRD analysis this observation was related to steric effects that provoked a reduction of the free channel passage inside the zeolite framework. Consequently some of the micropores of the H-ZSM5 zeolite were blocked as revealed by the decrease in the microporous surface area.

Temperature-programmed desorption of ammonia was used to characterise the overall acidity and the acid strength distribution of the catalysts (Fig. 3). On-line MS analysis confirmed that  $NH_3$  was the only species in the exit stream. Thus, the possibility of  $NH_3$  combustion over metal catalysts was ruled out. The area under the curve gave an estimation of the total amount of acid sites in each sample (Table 2). It was noticed that the acidity of the samples containing up to  $26\ wt.\% CeO_2$  ( $484$ – $558\ \mu mol\ NH_3\ g^{-1}$ ) was relatively similar to that of the bare support ( $490\ \mu mol\ NH_3\ g^{-1}$ ). Even a slight

**Table 1**  
Textural properties of the CeO<sub>2</sub>/H-ZSM5 zeolite catalysts.

Catalyst	S <sub>BET</sub> (m <sup>2</sup> g <sup>-1</sup> )	S <sub>EXT</sub> (m <sup>2</sup> g <sup>-1</sup> )	S <sub>micro</sub> (m <sup>2</sup> g <sup>-1</sup> )	V <sub>meso</sub> (cm <sup>3</sup> g <sup>-1</sup> )	V <sub>micro</sub> (cm <sup>3</sup> g <sup>-1</sup> )	d <sub>CeO<sub>2</sub></sub> (nm)
H-ZSM5	464	58	406	0.086	0.157	–
CeO <sub>2</sub> (6)/H-ZSM5	428	58	370	0.073	0.155	6.3
CeO <sub>2</sub> (11)/H-ZSM5	422	58	364	0.099	0.138	7.6
CeO <sub>2</sub> (17)/H-ZSM5	405	49	356	0.096	0.129	9.0
CeO <sub>2</sub> (26)/H-ZSM5	391	67	324	0.151	0.123	9.8
CeO <sub>2</sub> (50)/H-ZSM5	270	58	212	0.220	0.075	9.9
CeO <sub>2</sub>	99	–	–	0.210	–	9.0

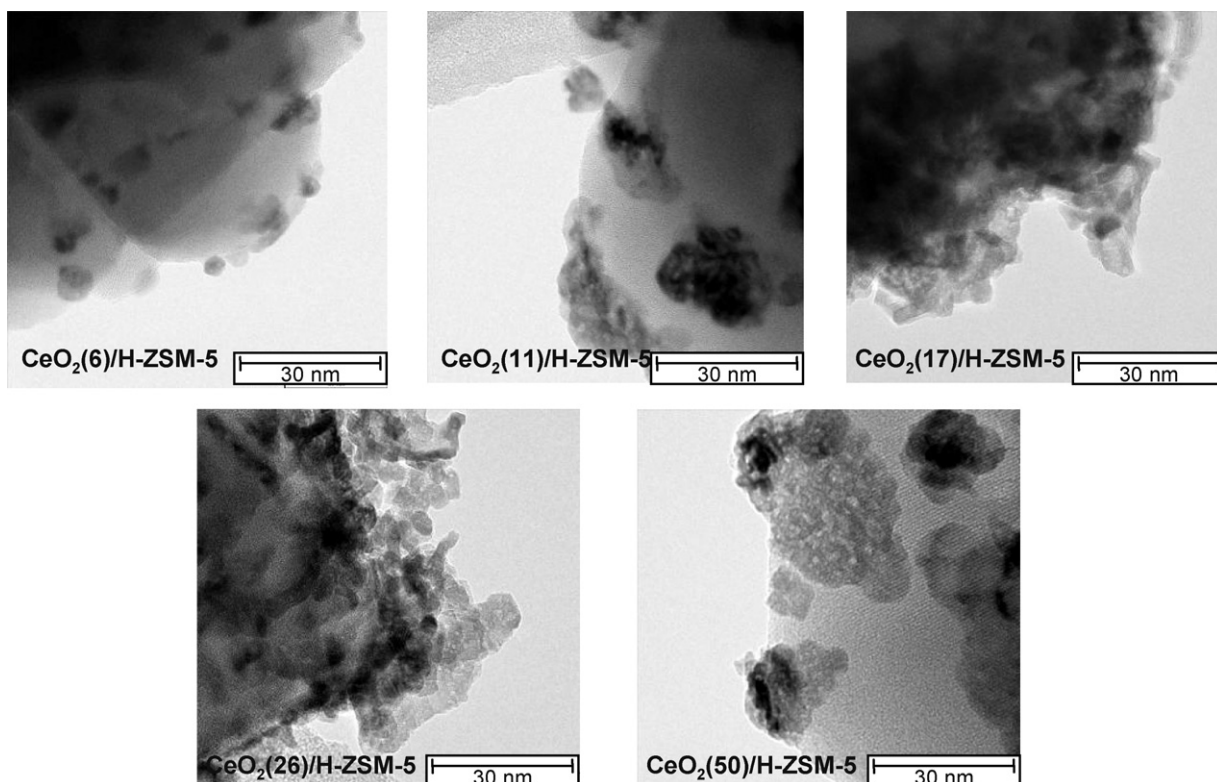


**Fig. 2.** TEM images of the CeO<sub>2</sub>/H-ZSM5 zeolite catalysts.

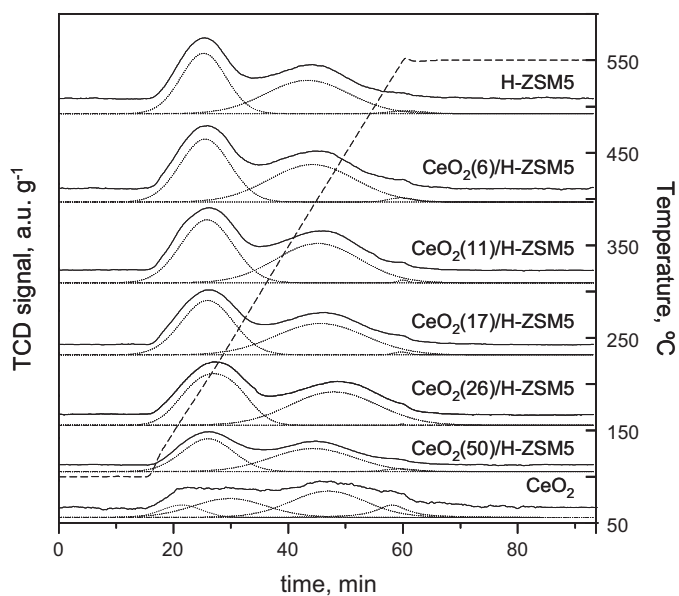


**Fig. 3.** NH<sub>3</sub>-TPD profiles of the CeO<sub>2</sub>/H-ZSM5 zeolite catalysts.

increase was observed in some cases (6 and 11 wt.%CeO<sub>2</sub>) probably due to the contribution of the inherent acidity of the deposited small CeO<sub>2</sub> crystallites. Note that pure ceria was characterised by a substantial overall acidity (about 110 μmol NH<sub>3</sub> g<sup>-1</sup>). As for the CeO<sub>2</sub>(50)/H-ZSM5 sample the acidity notably decreased owing to the major loss of surface area as a result of pore blockage [22]. In general, the TPD curves presented two distinct desorption peaks. The first peak that appeared at approximately 200 °C, was indicative of the presence weak sites, whereas the second one, located at around 380 °C, could be related to the presence of strong acid sites. In order to quantify the number of acid sites the profiles were deconvoluted into two Gaussian-like peaks (exceptionally

**Table 2**  
Acidic properties of the CeO<sub>2</sub>/H-ZSM5 zeolite catalysts.

Catalyst	Total acidity (μmol NH <sub>3</sub> g <sup>-1</sup> )	Weak acidity (%)	Strong acidity (%)
H-ZSM5	490	49	51
CeO <sub>2</sub> (6)/H-ZSM5	558	49	51
CeO <sub>2</sub> (11)/H-ZSM5	562	50	50
CeO <sub>2</sub> (17)/H-ZSM5	491	50	50
CeO <sub>2</sub> (26)/H-ZSM5	484	50	50
CeO <sub>2</sub> (50)/H-ZSM5	323	46	54
CeO <sub>2</sub>	112	40	60

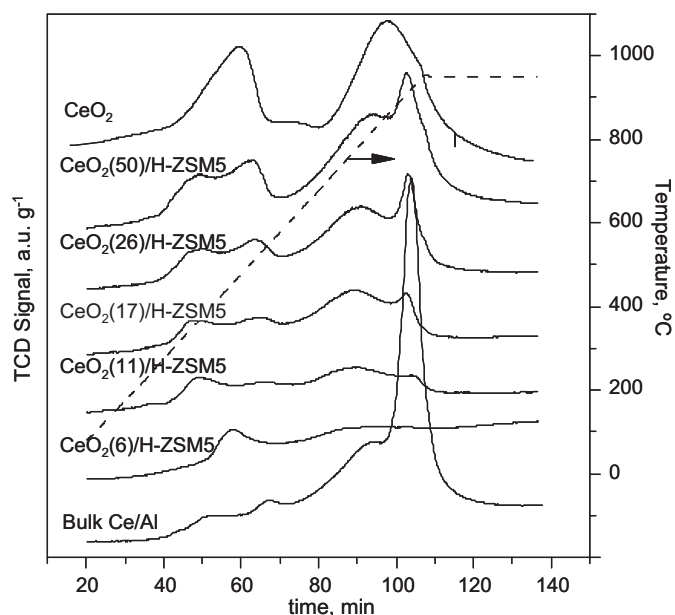


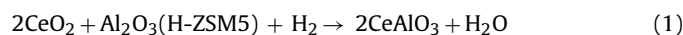
Fig. 4. H<sub>2</sub>-TPR profiles of the CeO<sub>2</sub>/H-ZSM5 zeolite catalysts.

the profile corresponding to pure ceria was deconvoluted into four Gaussian-like peaks). It was noticed that the acid strength distribution (relative amount of weak and strong acidity) was hardly modified by CeO<sub>2</sub> deposition, and that it was about 1:1 (virtually identical for all supported samples). It should be also pointed out that no evident change of peak temperatures in TPD profiles was noticed. This observation was in line with the results reported by Sugi et al. [22]. Previous results on pyridine adsorption followed by DRIFTS evidenced that H-ZSM5 zeolites contained both types of acid sites (Brønsted and Lewis), but predominantly Brønsted sites [11,23,24]. In contrast, the cerium pure oxide presented Lewis acid sites [25].

Cerium oxide is characterised by its oxygen storage capacity as a result of its facile redox system (Ce<sup>4+</sup>/Ce<sup>3+</sup>). The redox properties of the catalysts were thus examined by TPR with hydrogen. Fig. 4 shows the TPR profiles of CeO<sub>2</sub>/H-ZSM5 catalysts along with that of pure ceria. It could be seen that the pure CeO<sub>2</sub> sample displayed a broad reduction profile with a low-temperature H<sub>2</sub> peak centred at around 480 °C, which was attributed to the reduction of the uppermost layers of Ce<sup>4+</sup>, and a high-temperature H<sub>2</sub> peak centred at 870 °C approximately, which was associated with the bulk ceria reduction [5]. Note that no appreciable hydrogen consumption was observed for the parent H-ZSM5 zeolite (not shown in Fig. 4). As for the eventual presence of Ce<sup>3+</sup> in calcined CeO<sub>2</sub>/H-ZSM5 samples it was assumed that this could be considered negligible. In this sense, Martínez-Arias et al. [26] established a model of the characteristics of ceria entities present in CeO<sub>2</sub>/γ-Al<sub>2</sub>O<sub>3</sub> samples with a varying ceria content (1–39 wt.%). A multi-technique approach evidenced that ceria entities mostly contained Ce as Ce<sup>4+</sup>.

For the ceria supported catalysts the reduction of surface Ce<sup>4+</sup> present in dispersed ceria crystallites was seen to occur at slightly lower temperatures (250 °C) as compared with pure ceria (300 °C). However, in this case two reduction peaks instead of a single one were clearly visible at 400 and 500 °C, respectively. Also two reduction peaks were noticeable in the high-temperature range (>650 °C). These two peaks were tentatively assigned to the reduction of bulk ceria (800 °C) and the reduction of Ce<sup>4+</sup> to form bulk CeAlO<sub>3</sub> phase (950 °C) [27–31]. It is believed that CeAlO<sub>3</sub> may be formed by the partial reaction of cerium with aluminium (probably extraframework aluminium) from the zeolite under reductive conditions. The extent of this transformation was observed to be larger

with increasing cerium loading. In an attempt to verify the formation of cerium aluminate during the TPR run a bulk Ce/Al sample was synthesised according to the following procedure. An aqueous mixture of cerium nitrate and aluminium nitrate with a Ce:Al molar ratio of 1 was prepared. The solution was dried at 110 °C and the solid was then calcined at 550 °C in static air. Subsequently the sample was submitted to a temperature-programmed reduction under the same experimental conditions. The TPR profile of this sample is included in Fig. 4 and revealed a noticeable H<sub>2</sub> consumption in the 900–950 °C window according to the following reaction



XRD analysis of this reduced (uniformly green in colour) sample revealed the formation of CeAlO<sub>3</sub> (JCPDS 28-0260) with distinct diffraction lines at  $2\theta$  23.6°, 33.6° and 41.5° [32]. Note that most of the peaks corresponding to CeAlO<sub>3</sub> either overlap on or are very close to those of CeO<sub>2</sub>. The CeO<sub>2</sub>(26)/H-ZSM5 and CeO<sub>2</sub>(50)/H-ZSM5 samples after TPR were analysed by XRD in order to detect the formation of CeAlO<sub>3</sub>. Apparently, the main diffraction peaks of this species were not observed probably due to its relatively reduced formation and/or small crystallite size.

The amount of H<sub>2</sub> consumed during reduction was evidently larger with CeO<sub>2</sub> loading on the supported catalysts (Table 3). The CeO<sub>2</sub>(11)/H-ZSM5 sample exhibited the largest hydrogen uptake per gram of cerium. This involved a promoted Ce<sup>4+</sup> reduction between 350 and 550 °C. The values of H<sub>2</sub> consumption, which is a direct measurement of the amount of oxygen evolved from the sample, are useful for calculating the amount of Ce<sup>3+</sup> formed during reduction ( $n_{\text{Ce}^{3+}}$ ) [33]. The values of the percentage of Ce<sup>3+</sup> (%Ce<sup>3+</sup>) referred to the cationic sublattice are estimated according to the following equation

$$\% \text{Ce}^{3+} = \frac{n_{\text{Ce}^{3+}}}{n_{\text{Ce}_T}} \times 100 \quad (2)$$

where  $n_{\text{Ce}_T}$  is the amount of cerium ions in 1 mol of the oxide ( $n_{\text{Ce}_T}$  is equal to 1 for CeO<sub>2</sub>) is equal to 1 for CeO<sub>2</sub>). On the other hand, since the stoichiometry of the reduction process establishes that the formation of two Ce<sup>3+</sup> ions corresponds to the simultaneous formation of one oxygen vacancy [34], the amount of oxygen vacancies ( $n_{\text{OV}}$ ) in 1 mol of oxide can be therefore calculated as

$$n_{\text{OV}} = \frac{n_{\text{Ce}^{3+}}}{2} \quad (3)$$

The percentage of oxygen vacancies (%OV) corresponds to the percentage of vacancies present in the sample, with the anionic sublattice as a reference. This is equal to

$$\% \text{OV} = \frac{n_{\text{OV}}}{n_{\text{OT}}} \times 100 \quad (4)$$

where  $n_{\text{OT}}$  is the amount of oxygen sites in 1 mol of oxide. As  $n_{\text{OT}}$  is equal to 2 (2 mol of oxygen sites for 1 mol of oxide), from Eqs. (2)–(4), the percentage of oxygen vacancies referred to the total amount of oxygen atoms initially present in the oxide can be obtained as follows

$$\% \text{OV} = \frac{\% \text{Ce}^{3+}}{4} \quad (5)$$

The %OV is an interesting parameter to discuss on the basis of the labile oxygen for the catalytic reaction since it represents the amount of oxygen available for the catalytic oxidation of the chlorinated molecules [7]. Table 3 lists the %OV values after the reduction process up to 350 and 550 °C. The CeO<sub>2</sub>(11)/H-ZSM5 catalyst showed the highest values at both low and high reduction temperatures.

**Table 3**  
Redox properties of the CeO<sub>2</sub>/H-ZSM5 zeolite catalysts.

Catalyst	H <sub>2</sub> consumption (μmol H <sub>2</sub> g cat <sup>-1</sup> )		H <sub>2</sub> consumption (μmol H <sub>2</sub> g CeO <sub>2</sub> <sup>-1</sup> )		%OV	
	350 °C	550 °C	350 °C	550 °C	350 °C	550 °C
H-ZSM5	–	–	–	–	–	–
CeO <sub>2</sub> (6)/H-ZSM5	4.56	78.8	76.1	1312.5	0.65	11.3
CeO <sub>2</sub> (11)/H-ZSM5	18.53	160.0	168.4	1454.9	1.45	12.52
CeO <sub>2</sub> (17)/H-ZSM5	24.64	160.9	145.0	946.4	1.25	8.14
CeO <sub>2</sub> (26)/H-ZSM5	26.41	198.4	110.0	826.8	0.95	7.12
CeO <sub>2</sub> (50)/H-ZSM5	33.75	293.6	68.9	599.2	0.59	5.16
CeO <sub>2</sub>	40.05	344.1	40.0	344.1	0.34	2.96

### 3.2. Catalytic activity

The oxidation of 1,2-dichloroethane at constant weight hourly space velocity (635 g h mol<sub>DCE</sub><sup>-1</sup>) and feed concentration (1000 ppm in air) was chosen as a measure to evaluate the performance of the synthesised catalysts. Typically, catalytic activity was characterised by monitoring the rise in conversion as a function of temperature under given test conditions. A characteristic curve, referred to as the light-off or ignition curve, was obtained. *T*<sub>50</sub> (temperature at which 50% conversion was reached) was used as an indicative of the relative reactivity of the catalysts. Fig. 5 shows the light-off curves of the various H-ZSM5 supported ceria catalysts. Also the curves corresponding to the plain H-ZSM5, pure CeO<sub>2</sub> and CeAlO<sub>3</sub> were included for the sake of comparison. These samples were previously subjected to a calcination procedure similar to that of the supported catalysts. The possibility of homogeneous gas phase reactions at the reaction temperature range studied was checked through an experiment placing crushed quartz into the reactor tube. It was found that all the catalysed reactions needed lower reaction temperatures than the homogenous reaction (>400 °C) irrespective of the catalyst examined.

The bare zeolite exhibited a noticeably better conversion with respect to the pure cerium oxide (with a shift of about 100 °C). This highly active behaviour suggested that acidity played a relevant role in the activation of the reactant molecule [14]. However, as will be shown later, a disadvantage of plain H-ZSM5 as a catalyst for the oxidation of DCE is that CO is formed, while CO<sub>2</sub> is preferred,

and that it will lose its activity by deposition of carbonaceous material [11]. Interestingly, the addition of CeO<sub>2</sub> to the zeolitic support significantly increased the activity for DCE oxidation, decreasing *T*<sub>50</sub> from 250 to 210 °C (Table 4). This suggested a beneficial synergy between CeO<sub>2</sub> species and H-ZSM5 zeolite for the activation of oxygen species of the ceria crystallites [35]. Thus it is believed that the reaction was markedly accelerated owing to the simultaneous participation of the acid (mostly Brønsted-type) sites of the zeolite (where the chlorinated feed was efficiently adsorbed) and the redox sites from the metal phase (oxidation of the adsorbed feed with lattice oxygen anions) [6]. Although it could be a priori expected that increasing amounts of CeO<sub>2</sub> would lead to increasing activity of the catalysts, results included in Fig. 5 evidenced that there was an optimum Ce content (11 wt.%) for the investigated H-ZSM5 supported catalysts. Furthermore the activity of the CeO<sub>2</sub>/H-ZSM5 catalysts was essentially independent of the Ce loading over the range 26–50 wt.%. On the hand, it must be pointed out that the catalytic activity of CeAlO<sub>3</sub> was markedly lower in comparison with CeO<sub>2</sub> and ZSM-5 based catalysts with *T*<sub>50</sub> and *T*<sub>90</sub> of 385 and 450 °C, respectively.

From the characterisation results it is thought that the catalytic activity is governed by the degree of Ce<sup>4+</sup> reduction at low temperatures, which in turn depends on the crystallite size, along with the acidity of the resulting catalyst. The optimal combination of these features appears to be achieved for the sample CeO<sub>2</sub>(11)/H-ZSM5. In an attempt to clarify the influence of these two key catalytic properties of the zeolite supported ceria catalysts Figs. 6 and 7 illustrate the relationship between the catalytic activity (in terms of *T*<sub>50</sub>) and the %OV parameter and the overall acidity, respectively. From these graphs it is clearly observed that an effective oxygen mobility via Ce<sup>4+</sup> → Ce<sup>3+</sup> is more crucial for a high catalytic activity provided that deposition of CeO<sub>2</sub> does not lead to a substantial decrease in the intrinsic acidity of the zeolite support.

### 4. Product distribution

High conversion is not the only criterion for determining good chlorinated VOC destruction catalysts. It is indeed useful to provide some basic information about the nature and the amount of reaction products, as the combustion of chlorinated VOCs may be accompanied by the concomitant production of carbon monoxide and highly chlorinated by-products,

**Table 4**  
*T*<sub>50</sub> values (°C) for DCE oxidation over the CeO<sub>2</sub>/H-ZSM5 zeolite catalysts.

Catalyst	<i>T</i> <sub>50</sub> (°C)	<i>T</i> <sub>90</sub> (°C)
H-ZSM5	250	290
CeO <sub>2</sub> (6)/H-ZSM5	225	260
CeO <sub>2</sub> (11)/H-ZSM5	210	260
CeO <sub>2</sub> (17)/H-ZSM5	225	270
CeO <sub>2</sub> (26)/H-ZSM5	230	270
CeO <sub>2</sub> (50)/H-ZSM5	230	275
CeO <sub>2</sub>	320	395
CeAlO <sub>3</sub>	385	450

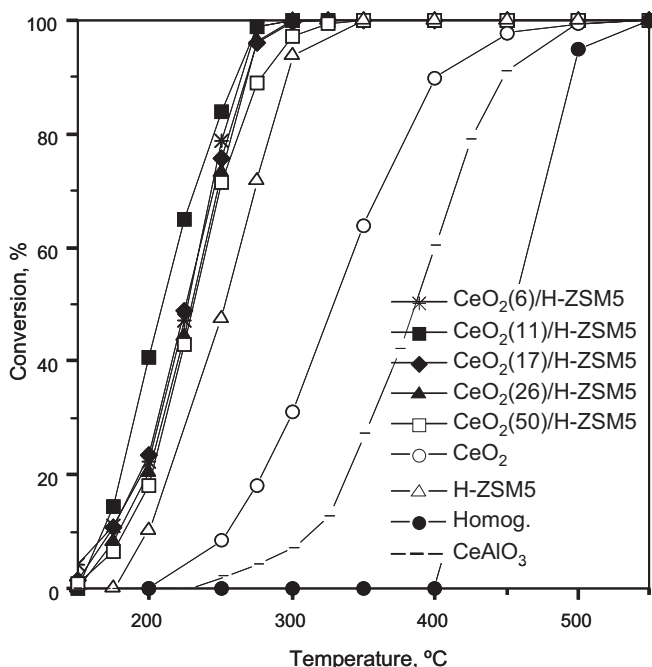


**Fig. 5.** Light-off curves of DCE oxidation over the CeO<sub>2</sub>/H-ZSM5 zeolite catalysts.

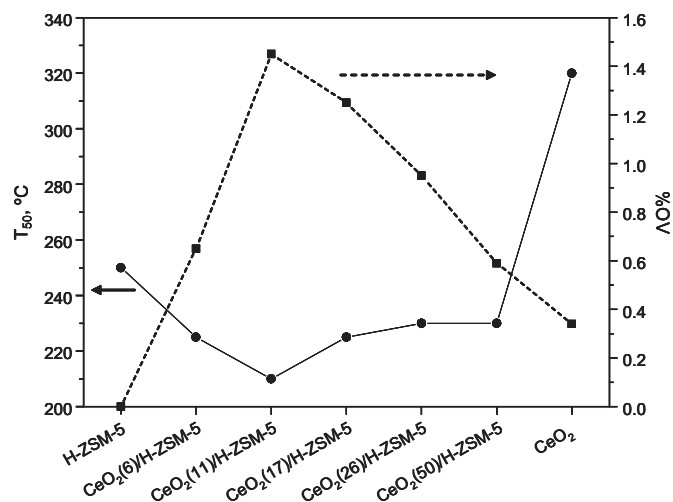


Fig. 6. Relationship between  $T_{50}$  and %OV for the CeO<sub>2</sub>/H-ZSM5 zeolite catalysts.

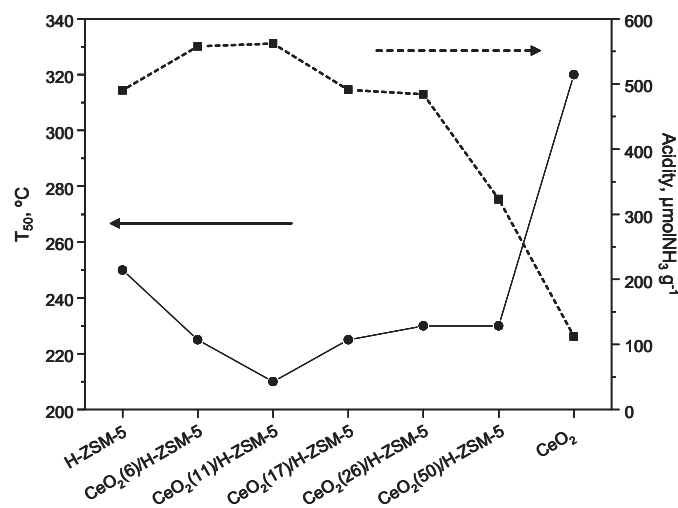
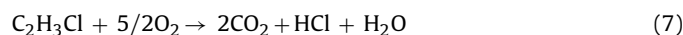


Fig. 7. Relationship between  $T_{50}$  and overall acidity for the CeO<sub>2</sub>/H-ZSM5 zeolite catalysts.

sometimes more toxic and recalcitrant than the starting material. DCE oxidation gave rise to CO<sub>2</sub>, CO, HCl and Cl<sub>2</sub> as major products. Nevertheless, the decomposition was accompanied by the generation of methyl chloride and vinyl chloride at mild temperatures (between 175 and 375 °C) according to Eqs. (6)–(9) (Fig. 8). These chlorinated intermediates were formed by partial oxidation and dehydrochlorination of the feed molecule, respectively. The peak concentrations were 200–225 ppm (200 °C) for methyl chloride and 100–120 ppm (250 °C) for vinyl chloride. In addition, reduced quantities (<20 ppm) of *trans*-1,2-dichloroethylene, *cis*-1,2-dichloroethylene, trichloroethylene and tetrachloroethylene were also identified. Other authors found acetic acid and acetaldehyde in the product stream over CeO<sub>2</sub>/Y catalysts [36], which was consistent with the proposed mechanism for DCE oxidation [25]. However, these species were not detected in our experiments probably due to the high activity of the examined catalysts for the oxidation of these compounds to yield carbon oxides and hydrogen chloride/molecular chlorine.



Apart from enhancing DCE conversion, which could be ranked as moderate, the deposition of CeO<sub>2</sub> crystallites on the zeolitic support resulted in slightly lower amounts of chlorinated by-products. What was more important was that these were abated at significantly lower temperatures. Note that the deep decomposition of the by-products generated over H-ZSM5 required temperatures higher than 450–500 °C. In addition, the increased yield of vinyl chloride can cause deactivation by coking, as it can readily polymerise to form carbonaceous residues [11].

At 350 °C, where DCE decomposition was almost complete (>99%) over the supported catalysts and the yield of chlorinated by-products was appreciably low (<10 ppm), the chlorine atoms present in the feed were preferentially converted into hydrogen chloride leading to HCl selectivity values higher than 90% over CeO<sub>2</sub>(6)/H-ZSM5, CeO<sub>2</sub>(11)/H-ZSM5 and CeO<sub>2</sub>(17)/H-ZSM5 catalysts (Table 5). In contrast, the selectivity decreased to 80% over CeO<sub>2</sub>(25)/H-ZSM5 and 72% over CeO<sub>2</sub>(50)/H-ZSM5. If the reaction temperature is increased the formation of hydrogen chloride is inhibited in favour of molecular chlorine. This observation was a

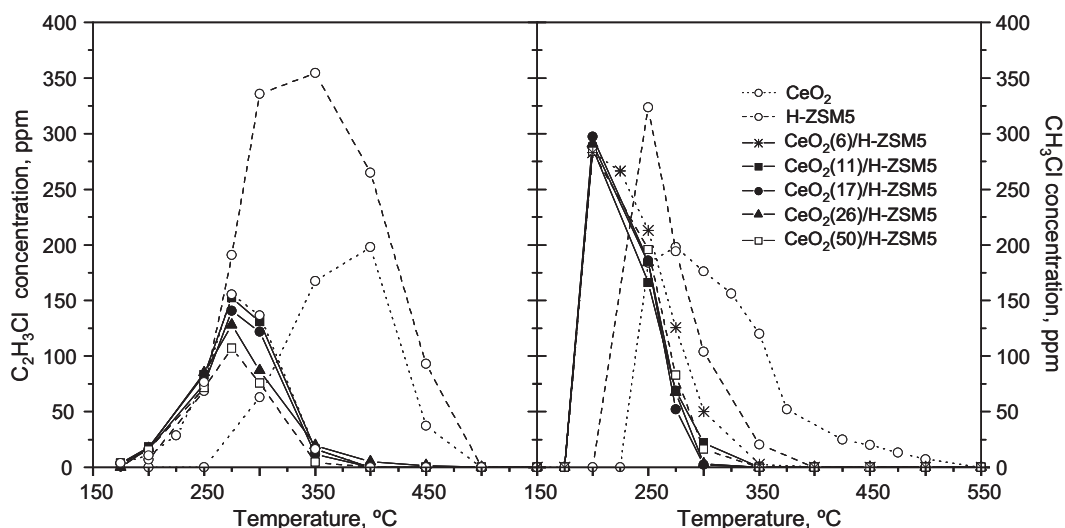
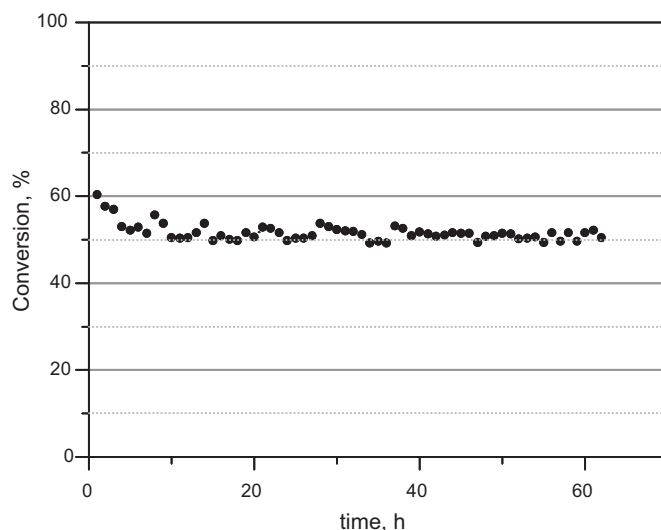


Fig. 8. Vinyl chloride and methyl chloride concentration profiles over the CeO<sub>2</sub>/H-ZSM5 zeolite catalysts.

**Table 5**  
Selectivity values (%) to CO<sub>2</sub>, CO, HCl and Cl<sub>2</sub> over the CeO<sub>2</sub>/H-ZSM5 zeolite catalysts as a function of temperature.

T (°C)	S <sub>HCl</sub>	S <sub>Cl<sub>2</sub></sub>	S <sub>CO<sub>2</sub></sub>	S <sub>CO</sub>
<b>CeO<sub>2</sub>(6)/H-ZSM5</b>				
250	54	0	17	4
300	70	0	29	66
350	95	3	30	70
400	68	32	33	67
500	47	53	39	61
550	56	44	49	51
<b>CeO<sub>2</sub>(11)/H-ZSM5</b>				
250	60	0	26	30
300	79	1	33	65
350	92	6	35	65
400	69	31	41	58
500	45	55	51	48
550	54	46	63	37
<b>CeO<sub>2</sub>(17)/H-ZSM5</b>				
250	55	1	18	35
300	73	1	27	70
350	91	6	27	72
400	66	34	32	68
500	46	54	43	57
550	50	50	56	44
<b>CeO<sub>2</sub>(26)/H-ZSM5</b>				
250	54	0	25	35
300	66	0	28	50
350	80	15	33	64
400	50	49	37	63
500	43	57	43	56
550	48	52	54	46
<b>CeO<sub>2</sub>(50)/H-ZSM5</b>				
250	42	0	25	33
300	57	8	30	57
350	72	18	41	58
400	49	51	43	56
500	45	55	54	46
550	48	52	66	34
<b>H-ZSM5</b>				
250	54	0	0	0
300	70	0	6	19
350	75	0	10	21
400	82	1	15	35
500	98	2	30	70
550	91	9	31	69
<b>CeO<sub>2</sub></b>				
250			7	1
300	37	18	10	3
350	27	25	25	7
400	27	30	52	17
500	41	58	68	24
550	40	60	70	30

consequence of the occurrence of the so-called Deacon reaction ( $2\text{HCl} + \text{O}_2 \leftrightarrow \text{Cl}_2 + \text{H}_2\text{O}$ ), which was activated at high temperatures mainly over ceria-rich supported catalysts. Thus, at 500–550 °C Cl<sub>2</sub> selectivity values as high as 55–60% were obtained over CeO<sub>2</sub>(26)/H-ZSM5 and CeO<sub>2</sub>(50)/H-ZSM5. On the other hand, all supported ceria catalysts converted DCE at 300–350 °C to give rise CO<sub>x</sub> as major carbon-containing oxidation products (Table 5). The relative CO/CO<sub>2</sub> ratio was about 70:30. At higher temperatures and metal content the oxidation of CO to CO<sub>2</sub> was favoured, and as a result significantly higher CO<sub>2</sub> selectivity values could be attained ranging from 50 to 66%. Note that CO<sub>2</sub> selectivity at 550 °C over plain H-ZSM5 was only 30%. In view of the results on the catalytic behaviour of CeO<sub>2</sub>/H-ZSM5 samples the main drawback of these catalysts is probably the high selectivity to CO instead of CO<sub>2</sub>. Adding water to the feedstream has been shown to be an efficient strategy to significantly increase the selectivity to CO<sub>2</sub> [37]. Another option could be that based on the addition of a second active metallic phase such as cobalt (with a known high activity for CO oxidation), but undesired side effects may appear, for example, an increase in Cl<sub>2</sub> yield (due to the occurrence of the Deacon



**Fig. 9.** DCE oxidation over CeO<sub>2</sub>(11)/H-ZSM5 sample at 225 °C as a function of time on stream.

reaction) and/or the formation of highly chlorinated by-products due to further chlorination of the feed [19].

## 5. Catalyst stability and characterisation of used samples

The stability of the most active sample, namely CeO<sub>2</sub>(11)/H-ZSM5, was investigated by analysing the evolution of conversion with time on stream at 225 °C for 80 h. This temperature was selected as it provoked a conversion of less than 100%, thus providing a more sensitive indication of changes of the catalyst performance with time on line. The used catalysts were characterised by BET measurements, dynamic thermogravimetry, XRD and EDX. A slight deactivation with a decrease in conversion from 60 to 51% was observed as shown in Fig. 9. The decline in conversion was evident during the initial 5 h interval while conversion remained reasonably stable at longer time on stream. This behaviour was in agreement with the results reported by Huang et al. [38] for the oxidation of DCE over CuO/CeO<sub>2</sub>/USY zeolite catalysts. Note that the generation of chlorinated by-products as well the selectivity to CO/CO<sub>2</sub> and HCl/Cl<sub>2</sub> remained unaffected with extended time on line.

Probably the deposition of coke, about 2 wt.% as quantified by thermogravimetry, was responsible for this decrease in activity. It is thought that the loss in activity caused by coking at longer time intervals was minimal because the amount of deposited coke was not increased with time. Probably there was a balance between the rate of coke formation (polymerisation of vinyl chloride) and the rate of partial coke combustion which could result in a constant accumulated amount of carbonaceous deposits. Hence, this balance was reflected by a lower but constant conversion. Note that coke started to oxidise, as revealed by dynamic thermogravimetry coupled to mass spectrometry, at about 175 °C. It was then reasonably to expect that combustion of coke may occur to a significant extent during DCE oxidation. TGA-MS analysis also revealed that these carbonaceous deposits could be completely burnt off at temperatures lower than 550 °C to yield CO<sub>2</sub> as deep oxidation product. This observation was important for the eventual regeneration step since it did not require excessively high temperatures which could induce a structural collapse of the zeolitic support and/or sintering of CeO<sub>2</sub> crystallites. On the other hand, the BET surface area of the spent catalyst was seen to decrease by 12%. XRD analysis revealed that the framework was preserved, thereby evidencing a relatively good

structural stability. Moreover, EDX analysis indicated the presence of a relatively reduced amount of Cl on the samples about 0.5 wt.%.

## 6. Conclusions

In this paper a series of H-ZSM5 supported CeO<sub>2</sub> samples with varying metallic loading (6–50 wt.%) were examined for the combustion of 1,2-dichloroethane, which is one of the most frequently chlorinated pollutants found in industrial processes. When compared with the plain support and the bulk cerium oxide the activity of the prepared catalysts was markedly higher irrespective of the cerium content. The combination of acidic and oxidising properties was responsible for their catalytic performance. From catalyst structure-activity relationships it could be established that catalytic activity was primarily governed by a more effective oxygen mobility of the deposited ceria crystallites. Overall acidity and acid strength distribution appeared to be of secondary importance. This bifunctional character was optimised for the supported sample with a CeO<sub>2</sub> content of 11 wt.%. This sample not only lowered the oxidation temperature, with a  $T_{50}$  value of 210 °C operating at 15,000 h<sup>-1</sup>, but also substantially reduced the formation of chlorinated intermediates, mainly vinyl chloride and methyl chloride. Interestingly, both chlorinated feed and by-products were abated at sufficiently low temperatures (<350 °C). As a consequence, the main chlorinated deep oxidation was hydrogen chloride instead of molecular chlorine since the Deacon reaction was not markedly activated. However, the main disadvantage was related to an incomplete selectivity to CO<sub>2</sub>. Finally, preliminary stability studies revealed that, although a certain decrease in conversion was noted mainly due to coking, the CeO<sub>2</sub>(11)/H-ZSM5 catalyst remained stable during 80 h time on line.

## Acknowledgements

The authors wish to thank the UPV/EHU-Gobierno Vasco (SAIOTEK S-PE11UN025) for the financial support. SGIker from Universidad del País Vasco/EHU is also gratefully acknowledged for EDX (Alfredo Sarmiento) and TEM (Gabriel López) analysis.

## References

- [1] Thematic Strategy on Air Pollution, Communication from the Commission to the Council and The European Parliament, Commission of the European Communities, COM (2005) 446 final, Brussels, 2005.
- [2] E.C. Moretti, Practical Solutions for Reducing Volatile Organic Compounds and Hazardous Air Pollutants, Centre for Waste Reduction Technologies of the American Institute of Chemical Engineers, New York, 2001.
- [3] J.J. Spivey, in: G. Ertl (Ed.), Handbook of Heterogeneous Catalysis, vol. 5, Wiley-VCH Verlag, Weinheim, 2008, pp. 2394–2411.
- [4] S. Pitkaaho, S. Ojala, T. Maunula, A. Savimaki, T. Kinnunen, R.L. Keiski, Appl. Catal. B 102 (2011) 395–403.
- [5] J.I. Gutiérrez-Ortiz, B. de Rivas, R. López-Fonseca, J.R. González-Velasco, Appl. Catal. A 269 (2004) 147–155.
- [6] J.I. Gutiérrez-Ortiz, B. de Rivas, R. López-Fonseca, J.R. González-Velasco, Appl. Catal. B 65 (2006) 191–200.
- [7] B. de Rivas, R. López-Fonseca, C. Sampedro, J.I. Gutiérrez-Ortiz, Appl. Catal. B 90 (2009) 545–555.
- [8] B. de Rivas, R. López-Fonseca, M.A. Gutiérrez-Ortiz, J.I. Gutiérrez-Ortiz, Appl. Catal. B 101 (2011) 317–325.
- [9] Q. Dai, X. Wang, G. Lu, Appl. Catal. B 81 (2008) 192–202.
- [10] R.W. van den Brink, P. Mulder, R. Louw, G. Sinquin, C. Petit, J.P. Hindermann, J. Catal. 180 (1998) 153–160.
- [11] R. López-Fonseca, A. Aranzabal, P. Steltenpohl, J.I. Gutiérrez-Ortiz, J.R. González-Velasco, Catal. Today 62 (2000) 367–377.
- [12] R. López-Fonseca, J.I. Gutiérrez-Ortiz, J.R. González-Velasco, Appl. Catal. A 271 (2004) 39–46.
- [13] R. López-Fonseca, J.I. Gutiérrez-Ortiz, M.A. Gutiérrez-Ortiz, J.R. González-Velasco, Catal. Today 107–108 (2005) 200–207.
- [14] J.I. Gutiérrez-Ortiz, R. López-Fonseca, U. Aurrekoetxea, J.R. González-Velasco, J. Catal. 218 (2003) 148–154.
- [15] S. Scirè, S. Minicò, C. Crisafulli, Appl. Catal. B 45 (2003) 117–125.
- [16] R. Rachapudi, P.S. Chintawar, H.L. Greene, J. Catal. 185 (1999) 58–72.
- [17] K.S. Go, Y. Kim, S.R. Son, S.D. Kim, Chem. Eng. Sci. 65 (2010) 499–503.
- [18] W.H.O. Regional Office for Europe, Air Quality Guidelines, second ed., WHO Regional Publications, European Series, Copenhagen, 2000, Chapter 5.6, No. 91.
- [19] B. de Rivas, R. López-Fonseca, C. Jiménez-González, J.I. Gutiérrez-Ortiz, J. Catal. 281 (2011) 88–97.
- [20] Y. Sugi, Y. Kubota, K. Komura, N. Sugiyama, M. Hayashi, J.-H. Kim, G. Seo, Appl. Catal. A 299 (2006) 157–166.
- [21] T. Dhannia, S. Jayalekshmi, M.C. Santhosh Kumar, T. Prasada Rao, A. Chandra Bose, J. Phys. Chem. Solid 70 (2009) 1443–1447.
- [22] Y. Sugi, Y. Kubota, K. Komura, N. Sugiyama, M. Hayashi, J.-H. Kim, Stud. Surf. Sci. Catal. 158 (2005) 1279–1286.
- [23] T. Armaroli, L.J. Simon, M. Digne, T. Montanari, M. Bevilacqua, V. Valtchev, J. Patarin, G. Busca, Appl. Catal. A 306 (2006) 78–84.
- [24] C. Costa, I.P. Dzikh, J.M. Lopes, F. Lemos, F. Ramoa Ribeiro, J. Mol. Catal. A 154 (2000) 193–201.
- [25] B. de Rivas, R. López-Fonseca, J.R. González-Velasco, J.I. Gutiérrez-Ortiz, J. Mol. Catal. A 278 (2007) 181–188.
- [26] A. Martínez-Arias, M. Fernández-García, L.N. Salamanca, R.X. Valenzuela, J.C. Conesa, J. Soria, J. Phys. Chem. B 104 (2000) 4038–4046.
- [27] S. Damyanova, C.A. Perez, M. Schmal, J.M.C. Bueno, Appl. Catal. A 234 (2002) 271–282.
- [28] A. Piras, S. Colussi, A. Trovarelli, V. Sergo, J. Llorca, R. Psaro, L. Sordelli, J. Phys. Chem. B 109 (2005) 11110–11118.
- [29] A.S. Prakash, C. Shivakumara, M.S. Hegde, Mater. Sci. Eng. B 139 (2007) 55–61.
- [30] L.F. Liotta, A. Longo, G. Pantaleo, G. Di Carlo, A. Martorana, S. Cimino, G. Russo, G. Deganello, Appl. Catal. B 90 (2009) 470–477.
- [31] L. Katta, G. Thrimurthulu, B.M. Reddy, M. Muhler, W. Grunert, Catal. Sci. Technol. 1 (2011) 1645–1652.
- [32] S.T. Aruna, N.S. Kini, S. Shetty, K.S. Rajam, Mater. Chem. Phys. 119 (2010) 485–489.
- [33] A.I. Kozlov, D.H. Kim, A. Yezerets, P. Andersen, H.H. Kung, M.C. Kung, J. Catal. 209 (2002) 417–426.
- [34] A. Trovarelli, Catalysis by Ceria and Related Materials, Catalytic Science Series, vol. 2, Imperial College Press, London, 2002.
- [35] Q. Huang, X. Xue, R. Zhou, J. Hazard. Mater. 183 (2010) 694–700.
- [36] J. Zhou, L. Zhao, Q. Huang, R. Zhou, X. Li, Catal. Lett. 127 (2009) 277–284.
- [37] B. de Rivas, R. López-Fonseca, M.A. Gutiérrez-Ortiz, J.I. Gutiérrez-Ortiz, Chemosphere 75 (2009) 1356–1362.
- [38] Q. Huang, X. Xue, R. Zhou, J. Mol. Catal. A 344 (2011) 74–82.